Neutron scattering and the B_{1g} phonon in the cuprates

T. P. Devereaux
Department of Physics, George Washington University, Washington, D.C. 20052

A. Virosztek and A. Zawadowski
Institute of Physics and Research Group of the Hungarian Academy of Sciences, Technical University of Budapest, H-1521 Budapest, Hungary
and Research Institute for Solid State Physics, P.O. Box 49, H-1525 Budapest, Hungary

(Received 13 March 1998; revised manuscript received 10 December 1998)

The momentum-dependent line shape of the out-of-phase oxygen vibration as measured in recent neutron-scattering measurements is investigated. Starting from a microscopic coupling of the phonon vibration to a local crystal field, the phonon line shift and broadening is calculated as a function of transferred momentum in the superconducting state of $YBa_2Cu_3O_7$. The absolute magnitude of the shift is obtained as a function of momentum and is found to be in excellent agreement with experiment. It is shown that the anisotropy of the density of states, superconducting energy gap, and the electron-phonon coupling are all crucial in order to explain these experiments. [S0163-1829(99)09421-7]

Recently, attention has focused on the observance of a resonance at an energy near 41 meV in the neutron-scattering cross section obtained in both optimally doped and underdoped $YBa_2Cu_3O_{7-\delta}$. [1,2] It has been speculated that this resonance feature might hold the key to the pairing mechanism that underlies superconductivity in the cuprate materials. As such, this feature has been lavished with attention by many various theoretical proposals.[3] Earlier measurements had suggested that this resonance was related to a particular phonon vibration that occurs at nearly the same energy. This phonon consists of the out-of-phase c-axis vibration of the two oxygen O(2) and O(3) atoms in the CuO_2 plane. However, it was later clarified via kinematic analysis and polarized neutron studies that a magnetic and phononic contribution are both present and could be separated. Both peaks could be tracked as a function of temperature as well as scattered neutron momentum. The phonon peak[2] has received a much smaller amount of attention in comparison with the magnetic resonance.

Earlier Raman[4] and neutron-scattering[5] experiments have studied this particular phonon vibration in detail. Of all the Raman-active phonons measured in tetragonal superconductors, only this phonon does not transform according to the full symmetry (A_{1g}) of the lattice. Since this phonon obeys its own selection rules (B_{1g}) it can be unambiguously identified. From its Fano profile, the magnitude of the electron-phonon (e-ph) coupling seems to be particularly large for this phonon compared to other phonons measured in Raman scattering. Indeed from the Raman point of view, this phonon has also been lavished with attention.[6–9] In Ref. 6, a phenomenological form for the coupling was assumed and thus predictions concerning the absolute magnitude of the line shift could not be obtained. Moreover, a simplified momentum dependence of the coupling was assumed. Only Refs. 7, 8, and 9 specified a microscopic source of the coupling. In Refs. 7 and 8 the coupling was a result of the buckling of the Cu-O plane. On the other hand, Ref. 9 has addressed this coupling as arising through a local crystal electric field **E** that breaks the inversion symmetry locally around the Cu-O plane.[10] Here the absolute value of the coupling estimated from calculations of the electric field gave good agreement to the results obtained from Raman scattering studies. Neither theories made predictions about the momentum dependence of the phonon line shape.

Reference 2 showed that in the normal state the B_{1g} phonon does not show any appreciable dependence on the in-plane neutron's scattered momentum **q**. However in the superconducting state the phonon softened considerably for $\mathbf{q}=0$, in agreement with Raman measurements, while the effect became rapidly less pronounced with increasing q. Along the (1,1,0) direction in the Brillouin zone (BZ), the phonon hardened faster with increasing q than along the (1,0,0) direction. While these findings were related to anisotropies of the energy gap, density of states, and the e-ph coupling, an unambiguous determination of the importance of each effect could not be made. We therefore refocus attention on the phonon contribution to neutron scattering in an effort to provide a theoretical framework to better understand the contributions from various anisotropies. Using a microscopic coupling theory developed in Ref. 9, the momentum dependence of the phonon line shape will be used to determine the interplay of the anisotropies of the energy gap, density of states, and the e-ph coupling. An estimate for the magnitude of the line shape changes as a function of momentum can be obtained.

Our starting point is a three-band model for the CuO_2 plane with Cu-O hopping amplitude t and O-O hopping amplitude t':

$$H_0=\epsilon\sum_{\mathbf{n},\sigma} b^{\dagger}_{\mathbf{n},\sigma}b_{\mathbf{n},\sigma}+t\sum_{\mathbf{n},\sigma,\boldsymbol{\delta}}[P_{\boldsymbol{\delta}}b^{\dagger}_{\mathbf{n},\sigma}a_{\mathbf{n},\boldsymbol{\delta},\sigma}+\text{H.c.}]$$
$$+t'\sum_{\mathbf{n},\sigma}\sum_{\langle\boldsymbol{\delta},\boldsymbol{\delta}'\rangle}P'_{\boldsymbol{\delta},\boldsymbol{\delta}'}a^{\dagger}_{\mathbf{n},\boldsymbol{\delta},\sigma}a_{\mathbf{n},\boldsymbol{\delta}',\sigma}, \quad (1)$$

where $b^{\dagger}_{\mathbf{n},\sigma}$ creates an electron with spin σ at a copper lattice site **n**, while $a_{\mathbf{n},\boldsymbol{\delta},\sigma}$ annihilates an electron at one of the

neighboring oxygen sites $\mathbf{n}+\boldsymbol{\delta}/2$ determined by the unit vector $\boldsymbol{\delta}$ assuming the four values, $(\pm 1,0)$ and $(0,\pm 1)$. An oxygen atom between the two copper atoms at sites $\mathbf{n}$ and $\mathbf{n}+\boldsymbol{\delta}$ is labeled by either $(\mathbf{n},\boldsymbol{\delta})$ or $(\mathbf{n}+\boldsymbol{\delta},-\boldsymbol{\delta})$. As in Ref. 9, $\epsilon=E_d-E_p$ is the difference of the Cu and O site energies and $P_{\boldsymbol{\delta}}=\pm 1$, depending on whether the orbitals (with real wave functions) have the same or opposite sign at the overlap region. Assuming Cu $d_{x^2-y^2}$ and O p orbitals $P_{-\boldsymbol{\delta}}=-P_{\boldsymbol{\delta}}$, and we can choose $P_{(1,0)}=1$ and $P_{(0,1)}=-1$. Lastly, $P'_{\boldsymbol{\delta},\boldsymbol{\delta}'}$ denotes the overlap sign between an oxygen orbital at site $\mathbf{n}+\boldsymbol{\delta}/2$ with a neighboring oxygen orbital at site $\mathbf{n}+\boldsymbol{\delta}'/2$. The O-O hopping is needed to give the right curvature and centering of the observed Fermi surface. By our above convention these overlaps take the values $P'_{\mathbf{x},\mathbf{y}}=P'_{-\mathbf{x},-\mathbf{y}}=1$, and $P'_{\mathbf{x},-\mathbf{y}}=P'_{-\mathbf{x},\mathbf{y}}=-1$, respectively. After Fourier transforming, the Hamiltonian now reads $H^0=\Sigma_{\mathbf{k},\sigma}H^0_{\mathbf{k},\sigma}$, where

$$H^0_{\mathbf{k},\sigma}=\epsilon b^\dagger_{\mathbf{k},\sigma}b_{\mathbf{k},\sigma}+\{ib^\dagger_{\mathbf{k},\sigma}[a_{x,\mathbf{k},\sigma}t_x(\mathbf{k})-a_{y,\mathbf{k},\sigma}t_y(\mathbf{k})]+\text{H.c.}\}+t'(\mathbf{k})[a^\dagger_{x,\mathbf{k},\sigma}a_{y,\mathbf{k},\sigma}+\text{H.c.}], \tag{2}$$

with the prefactors $t_\alpha(\mathbf{k})=2t\sin(ak_\alpha/2), t'(\mathbf{k})=-4t'\sin(ak_x/2)\sin(ak_y/2)$. We can then diagonalize Eq. (2): $H^0_{\mathbf{k},\sigma}=\Sigma_\beta\epsilon_\beta(\mathbf{k})d^\dagger_{\beta,\mathbf{k},\sigma}d_{\beta,\mathbf{k},\sigma}$, where β is $+$, $-$, and 0 for the antibonding, bonding, and nonbinding bands, respectively. We consider only a reduced one band model appropriate near half filling and take only the upper band into account.[11] At this point the same procedure used in Ref. 9 can be carried through. The electric fields at the O(2) and O(3) sites couple linearly to their c-axis ion displacements leading to the following e-ph coupling:

$$H_{\text{e-ph}}=eE\hat{\mathbf{z}}\cdot\sum_{\mathbf{n},\sigma}\{\mathbf{u}_x(a\mathbf{n})a^\dagger_{\mathbf{n},\mathbf{x},\sigma}a_{\mathbf{n},\mathbf{x},\sigma}+\mathbf{u}_y(a\mathbf{n})a^\dagger_{\mathbf{n},\mathbf{y},\sigma}a_{\mathbf{n},\mathbf{y},\sigma}\}, \tag{3}$$

where E is the c-axis aligned electric field at the O(2) and O(3) sites, neglecting orthorhombic distortions. This can be rewritten in a momentum representation as

$$H_{\text{e-ph}}=\frac{1}{\sqrt{N}}\sum_{\mathbf{q},\mathbf{k},\sigma}g(\mathbf{k},\mathbf{q})d^\dagger_{\mathbf{k},\sigma}d_{\mathbf{k}-\mathbf{q},\sigma}[c_{\mathbf{q}}+c^\dagger_{-\mathbf{q}}], \tag{4}$$

where $c_{\mathbf{q}}$ annihilates the B_{1g} phonon mode with wave vector $\mathbf{q}$ and $g(\mathbf{k},\mathbf{q})$ is the coupling constant of the mode to an electron of wave vector $\mathbf{k}$.

The coupling constant for the $\mathbf{q}=0$ B_{1g} phonon was evaluated in Ref. 9. These results can be generalized for finite $\mathbf{q}$ as

$$g(\mathbf{k},\mathbf{q})=eE_z\sqrt{\frac{\hbar}{2M_{\text{O}}N(\mathbf{q})\omega_{B_{1g}}}}\times[\phi^*_x(\mathbf{k})\phi_x(\mathbf{k}-\mathbf{q})e^{-iq_xa/2}(1+e^{-iq_ya})-\phi^*_y(\mathbf{k})\phi_y(\mathbf{k}-\mathbf{q})e^{-iq_ya/2}(1+e^{-iq_xa})]. \tag{5}$$

Here M_{O} is the oxygen mass and $\omega_{B_{1g}}\sim 41$ meV is the phonon frequency. The ϕ functions result from the diagonalization of the three-band model and are given as

$$\phi_{x,y}(\mathbf{k})=\frac{\mp i}{N_{\mathbf{k}}}[t_{x,y}(\mathbf{k})-t'(\mathbf{k})t_{y,x}(\mathbf{k})/\epsilon(\mathbf{k})] \tag{6}$$

with the normalization factor

$$N_{\mathbf{k}}=\frac{1}{\epsilon(\mathbf{k})}\{[\epsilon(\mathbf{k})^2-t'(\mathbf{k})^2]^2+[\epsilon(\mathbf{k})t_x(\mathbf{k})-t_y(\mathbf{k})t'(\mathbf{k})]^2+[\epsilon(\mathbf{k})t_y(\mathbf{k})-t_x(\mathbf{k})t'(\mathbf{k})]^2\}^{1/2}. \tag{7}$$

Lastly, the exponential factors and the other normalization $N(\mathbf{q})$ comes from the phonon displacements. The eigenvalue and momentum-dependent eigenvector for the B_{1g} ionic vibration is solved for the simple harmonic model of the three-atom-unit cell of Cu coupled via identical spring constants K to both the O(2) and O(3) atoms under a uniform tension. Besides an acoustic mode and an in-phase O(2)-O(3) optical mode (A_{1g}), the B_{1g} mode is obtained with the dispersionless energy eigenvalue $\omega^2_{B_{1g}}=2K/M_{\text{O}}$, and whose eigenvector is

$$\boldsymbol{\epsilon}^{\text{O(2,3)}}_{B_{1g}}(\mathbf{q})=\pm\hat{\mathbf{z}}(1+e^{-iq_{y,x}a})/\sqrt{N(\mathbf{q})}, \tag{8}$$

$$N(\mathbf{q})=4[\cos^2(q_xa/2)+\cos^2(q_ya/2)].$$

The eigenvectors from this simplified model give an adequate agreement to the eigenvectors obtained via more complex lattice-dynamical calculations.[12]

The e-ph coupling renormalizes the bare phonon propagator $D^0_{B_{1g}}(\mathbf{q},\omega)=2\omega_{B_{1g}}/[\omega^2-\omega^2_{B_{1g}}]$ such that the retarded propagator becomes

$$D_{B_{1g}}(\mathbf{q},\omega+i\boldsymbol{\delta})=\frac{D^0_{B_{1g}}(\mathbf{q},\omega)}{1+D^0_{B_{1g}}(\mathbf{q},\omega)\Pi_{B_{1g}}(\mathbf{q},\omega+i\delta)}, \tag{9}$$

where $\Pi_{B_{1g}}$ is the $\mathbf{q}$ and ω dependent polarization,

$$\Pi_{B_{1g}}(\mathbf{q},\omega+i\delta)=\sum_{\mathbf{k}}|g(\mathbf{k},\mathbf{q})|^2\times\left\{a_+(\mathbf{k},\mathbf{q})[f(E_{\mathbf{k}})-f(E_{\mathbf{k}+\mathbf{q}})]\left(\frac{1}{\omega+i\delta+E_{\mathbf{k}}-E_{\mathbf{k}+\mathbf{q}}}-\frac{1}{\omega+i\delta-E_{\mathbf{k}}+E_{\mathbf{k}+\mathbf{q}}}\right)+a_-(\mathbf{k},\mathbf{q})[1-f(E_{\mathbf{k}})-f(E_{\mathbf{k}+\mathbf{q}})]\left(\frac{1}{\omega+i\delta-E_{\mathbf{k}}-E_{\mathbf{k}+\mathbf{q}}}-\frac{1}{\omega+i\delta+E_{\mathbf{k}}+E_{\mathbf{k}+\mathbf{q}}}\right)\right\}, \tag{10}$$

where $E_{\mathbf{k}}=\sqrt{\xi_{\mathbf{k}}^2+\Delta^2(\mathbf{k})}$, $\xi_{\mathbf{k}}=\epsilon(\mathbf{k})-\mu$ is the energy dispersion measured from the chemical potential μ, f is the Fermi function, and $a_{\pm}(\mathbf{k},\mathbf{q})$ are coherence factors,

$$a_{\pm}(\mathbf{k},\mathbf{q})=1\pm\frac{\xi_{\mathbf{k}}\xi_{\mathbf{k}+\mathbf{q}}-\Delta(\mathbf{k})\Delta(\mathbf{k}+\mathbf{q})}{E_{\mathbf{k}}E_{\mathbf{k}+\mathbf{q}}}. \tag{11}$$

This expression is identical to the one used in Ref. 6. However, all other uses of Eqs. (10) and (11) have used a momentum-independent coupling constant and have not specified a microscopic mechanism for the electron-phonon interaction. We remark here that this misses crucial information of the interplay of symmetry of the phonon vibration and its coupling to the electronic system. First of all, the use of **k**-independent coupling constant in Eqs. (10) and (11) corresponds to a particular case of a fully symmetric phonon (A_{1g}), transforming as the identity representation. As a consequence of the long-wavelength Coulomb interaction, the $\mathbf{q}=0$ self-energy would be completely screened, leading to no net linewidth change for $\mathbf{q}=0$ phonons, as measured, e.g., in Raman-scattering measurements.[9,13] If a fully symmetric phonon has a momentum dependence, it still will be at least partially screened by the long-wavelength Coulomb interaction. However, there is no screening for phonons of other symmetry. While it appears that certain A_{1g} phonons in the cuprates are weakly temperature dependent and may indeed have their coupling to the electron system screened out, the Ba A_{1g} phonon as well as the O B_{1g} vibration show distinctive shifts as a function of temperature. This can only come about if the phonons have a nontrivial momentum-dependent coupling constant and therefore the use of a momentum independent coupling constant is inappropriate for these phonons.[4] Second, the neglect of the momentum dependence of the coupling constant overestimates the size of the B_{1g} phonon broadening shift for $\mathbf{q}=0$. As with the electronic contribution to the Raman response,[14] the coupling of the gap and the vertex that have the same symmetry leads to a reduction of the phonon broadening in the superconducting state $\sim(\omega/2\Delta)^3$ compared to the case when the gap and vertex are of different symmetries $\sim\omega/\Delta$.[13] Lastly, the momentum dependence is not separable into two functions of **k** and **q**, respectively, as implied in Ref. 6.

Here we consider either an anisotropic s wave or $d_{x^2-y^2}$ energy gap: $\Delta_s(\mathbf{k})=\Delta_0|[\cos(k_xa)-\cos(k_ya)]|/2$, $\Delta_d(\mathbf{k})=\Delta_0[\cos(k_xa)-\cos(k_ya)]/2$. While we believe that there is strong evidence that the energy gap in the cuprates has $d_{x^2-y^2}$ symmetry, we consider the s-wave case for illustrative purposes showing the effect of a sign change of the energy gap. In the following we choose $\epsilon=1$ eV, $t=1.6$ eV, and $t'/t=0.45$ (which are similar to the values chosen in Ref. 8), $\Delta_0=30$ meV and $2\Delta_0/k_BT_c=8$ for both energy-gap choices, and $\omega=41$ meV. We adjust the chemical potential to yield a filling $\langle n\rangle=0.875$ for both spins, and set $T=T_c/2$.

In Fig. 1 we plot the real and imaginary parts of Π as a function of transferred momentum **q** along the (1,1,0) direction for a $d_{x^2-y^2}$ and an anisotropic s-wave superconductor, while Fig. 2 plots these same functions for **q** along the (1,0,0) direction. We have normalized both the real and imaginary parts of Π to their $\mathbf{q}=0$ values. The three factors governing the **q** dependence of the B_{1g} phonon's line shape

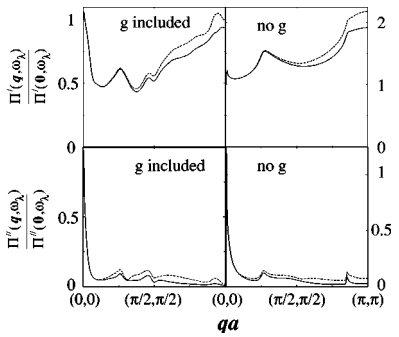

FIG. 1. Real and imaginary parts of the B_{1g} phonon self energy as a function of momentum transfer **q** along the BZ diagonal for $T=T_c/2$. The solid lines in the figures correspond to the $d_{x^2-y^2}$ energy gap and the long-dashed lines correspond to the $|d_{x^2-y^2}|$ energy gap. The left panels represent the evaluation of Eqs. (10) and (11) using the expression for the coupling constant g, Eq. (5), while the right panels correspond to using a momentum-independent coupling constant equal to t.

are the joint density of states for phonon scattering, the coherence factors, and the e-ph coupling.

We first consider features of the polarization Π that are only due to kinematic constraints and band structure. Starting from $q=0$, where Cooper pairs are broken equally around the Fermi surface (FS), the pair breaking becomes less resonant as q increases until two regions of the FS can be connected. At the same time the scattering processes at low temperatures that are most prominent are those that can most closely satisfy the condition that $\omega=|\Delta(\mathbf{k})|+|\Delta(\mathbf{k}+\mathbf{q})|$ coming from last term in Eq. (10). Both of these restrictions become less and less obeyed with increasing **q** and lead to a very rapid dropoff of Π away from $\mathbf{q}=0$ in either direction, as seen in both figures regardless of the energy-gap symmetry. Moreover, as **q** approaches the zone boundary along the diagonal (Fig. 1), both the real part of Π rises since regions of the FS with large density of states (flat bands) are connected by momentum transfer of $(\pi/a,\pi/a)$.

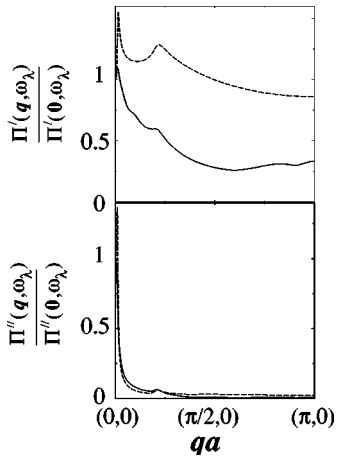

FIG. 2. Real and imaginary parts of the B_{1g} phonon self-energy as a function of momentum transfer **q** along the BZ axis for $T=T_c/2$. Both gap choices yield identical results. The solid lines in the figures correspond to evaluating Eqs. (10) and (11) using the expression for the coupling constant g, Eq. (5), while the dashed lines correspond to using a momentum-independent coupling constant equal to t.

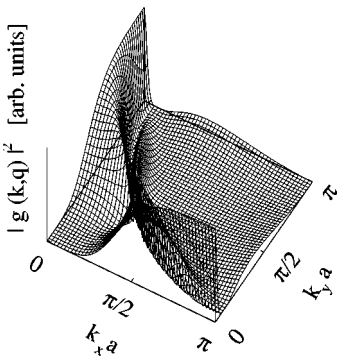

FIG. 3. The momentum dependence of the coupling constant $|g(\mathbf{k},\mathbf{q}=0)|^2$ as a function of momentum in the BZ.

Now if we consider the anisotropy of the energy gap, we note that for the anisotropic s-wave case this rise is more pronounced than the d-wave case due to the change of sign of the gap in the coherence factor a_- for the d-wave gap. As we would expect, there is no difference between Π evaluated for the two gaps for $\mathbf{q}$ transfer along the (1,0,0) direction since the coherence factor is the same for both energy gaps for scattering near the FS.

We now consider the momentum dependence of the coupling constant. In Fig. 1 (left panel) and Fig. 2 the solid line represents Π calculated with the coupling constant included while the right panel of Fig. 1 and the dashed lines in Fig. 2 are obtained by neglecting the **k,q** dependence of the coupling constant. We see that the results for both $\mathbf{q}$ directions are strongly affected by the coupling constant and its inclusion cannot be neglected. In all cases the coupling constant leads to a more rapid falloff of the polarization with increasing $\mathbf{q}$. This is due to the strong momentum dependence of the coupling constant $g(\mathbf{k},\mathbf{q})$. For $\mathbf{q}=0$, the vertex varies as $\sim[\cos(k_x a)-\cos(k_y a)][\epsilon(\mathbf{k})-t'(\mathbf{k})]$—it vanishes along the BZ diagonal and just off the FS when $t'(\mathbf{k})=\epsilon(\mathbf{k})$. This is seen in Figs. 3, 4, and 5, which plot the vertex for $\mathbf{q}=(0,0),(\pi/a,0)$, and $(\pi/a,\pi/a)$, respectively. Thus the vertex suppresses scattering just off the FS plus scattering between BZ diagonals, leading to the rapid falloff of Π with momentum transfer $\mathbf{q}$ as seen in Figs. 1 and 2. This is in general agreement with the results from Ref. 2, supporting the importance of the coupling constant.

Finally, we consider the absolute magnitude for the hardening of the B_{1g} phonon as a function of $\mathbf{q}$. By specifying

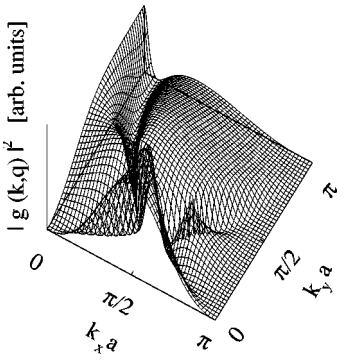

FIG. 4. The momentum dependence of the coupling constant $|g(\mathbf{k},\mathbf{q}=\pi/a,0)|^2$ as a function of momentum in the BZ.

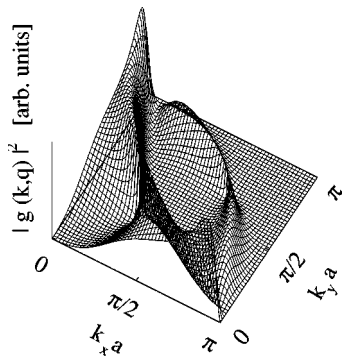

FIG. 5. The momentum dependence of the coupling constant $|g(\mathbf{k},\mathbf{q}=\pi/a,\pi/a)|^2$ as a function of momentum in the BZ.

the microscopic source of the e-ph coupling mechanism, we can provide a numerical check of the strength of the coupling. For this it is useful to examine the neutron-scattering cross section[15] for scattering by the B_{1g} phonon. The neutron-scattering cross section can be written as

$$\frac{d^2\sigma}{d\Omega\, d\omega}\sim|F(\mathbf{q})|^2 S(\mathbf{q},\omega), \tag{12}$$

where F is the form factor for scattering by the B_{1g} phonon, $S=\mathrm{Im}\,D$ [see Eq. (9)] is the phonon spectral function, and $\hbar\omega$ is the difference in energy of the scattered and incident neutron. As in Ref. 2, we consider umklapp scattering of the neutron by the phonon for momentum transfers of $\mathbf{Q}+\mathbf{q}$, where $\mathbf{Q}=(2\pi/a,0)$. This determines the form factor as

$$|F(\mathbf{q})|^2=\frac{[\cos(q_x a/2)+\cos(q_y a/2)]^2}{\cos^2(q_x a/2)+\cos^2(q_y a/2)}. \tag{13}$$

Using $\omega_{B_{1g}}=348\ \mathrm{cm}^{-1}$ and the magnitude of the Cu-O buckling, $eE_z=-0.8\ \mathrm{eV/\AA}$,[16] we plot in Fig. 6 the results for the cross section for a $d_{x^2-y^2}$ superconductor for $\mathbf{q}$ along the diagonal and axis of the BZ, respectively. The e-ph coupling has been included, and the parameters used are the same as for Fig. 2. In addition, a constant phonon linewidth of 2.5 cm^{-1} was included that represents the intrinsic broadening of the phonon (i.e., due to anharmonic lattice potentials), which is present even in the insulating state.[9] Once the spectral function was obtained the curve was convoluted with a

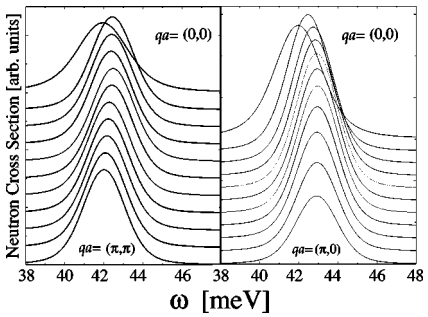

FIG. 6. The neutron cross section as a function of ω for different $\mathbf{q}$ values. The $\mathbf{q}$ values are chosen in equal increments along the diagonal (axis) of the BZ for the left (right) panel, respectively. Each curve has been offset for clarity.

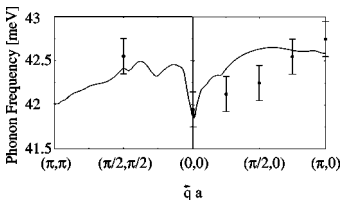

FIG. 7. Comparison of the theory with the experimental data of Ref. 2.

Gaussian of width 2 meV to mimic the experimental resolution of the apparatus used in Ref. 2.

Our results for the frequency shift of the phonon for different momenta are compared to the experimental data in Fig. 7 using the above parameters. We note that the theory compares both qualitatively and quantitatively well with the data in two regards. First, the theory predicts a hardening of the phonon for increasing momentum transfers in both directions in agreement with experiment (although data along the BZ diagonal is not very complete). Further, a maximum hardening of roughly 0.9 meV observed for momentum transfer along the BZ axis is in agreement with the measured[2] hardening of 0.9 ± 0.1 meV. The general behavior away from the zone center $(\mathbf{q}=0)$ is reproduced as well. As mentioned, the data along the BZ axis cannot be used to determined whether the energy gap changes sign, but we note that if the anisotropic *s* energy gap was used it would predict a larger growth of the shift along the BZ diagonals than displayed in Fig. 7.

Three important details of the data are not captured by the theory however. The theory gives a more abrupt falloff for the shift along the BZ axis than seen in the experiment, although a slightly larger error bar (as seen in two points in Ref. 2) would cover the discrepancy. The experimental data show large changes for the phonon frequency for $T=0.5T_c$ compared to $0.1T_c$, which the theory cannot reproduce. Lastly, if the theory is used to calculate the phonon frequency as a function of momentum in the normal state, the phonon develops dispersion that roughly tracks the dispersion seen in the superconducting state for momentum transfers larger than $\pi a/2$ in either direction. This is also in disagreement with the experiment, which shows a relatively dispersionless phonon above T_c.

These points may be indicative of the neglect of strong electronic correlations. The theory does not include the effects of strong electronic correlations as the electronic parameters are taken in accord with local-density-approximation values.[8] This may crucially affect the momentum dependence of the line shape as the momentum vector maps out the band dispersion as well as the shape of the Fermi surface. The strong local Coulomb repulsion would lead to a smaller renormalized bandwidth and thus a less rapid dependence of Π with momentum. The theory could be refined once parameter choices for the band structure are determined via fitting to experimentally determined band dispersion and Fermi surfaces. This remains to be investigated. The strong temperature dependence of the phonon even below T_c remains puzzling. All theory curves are essential T—independent below $T=0.5T_c$ as the energy gap is completely established. The phonon line shape changes below T_c are due to the opening of a phonon decay channel by breaking Cooper pairs near $\mathbf{q}=0$ and are minimized by momentum and energy conservation at larger momentum transfers. Additional scattering via, e.g., impurities or spin fluctuations, open channels for phonon scattering at small $\mathbf{q}$ in the normal state as well, which may counteract the dispersion given by Π. However, this cannot yield a strong temperature-dependent scattering substantially below T_c.

In summary we have investigated contributions to the momentum dependence of the B_{1g} phonon resulting from anisotropies of the density of states, energy gap, and *e*-ph coupling constant. Using a microscopic theory for the origin of the *e*-ph coupling as given in Ref. 9, the theory's prediction for the dependence of the line shape of the phonon as a function of $\mathbf{q}$ for various directions in the BZ is in qualitative agreement with the results of Ref. 2, while the magnitude of the hardening of the phonon is in quantitative agreement. It is crucial that the anisotropies of all quantities are taken into account.

T.P.D. would like to acknowledge helpful conversations with N. Bulut, D. Scalapino, R. T. Scalettar, T. Fong, D. Reznik, and B. Keimer. Acknowledgment is made to the Donors of The Petroleum Research Fund, administered by the American Chemical Society, for partial support of this research. This work was supported by the Hungarian National Research Fund under Grant Nos. OTKA T020030, T016740, T021228/1996, T024005/1997, and by the U.S.-Hungarian Joint Fund No. 587.

[1] H. A. Mook *et al.*, Phys. Rev. Lett. **70**, 3490 (1993); H. F. Fong *et al.*, *ibid.* **75**, 316 (1995); Phys. Rev. B **54**, 6708 (1996); Phys. Rev. Lett. **78**, 713 (1997).

[2] D. Reznik *et al.*, Phys. Rev. Lett. **75**, 2396 (1995).

[3] N. Bulut and D. J. Scalapino, Phys. Rev. B **47**, 3419 (1993); E. Demler and S.-C. Zhang, Phys. Rev. Lett. **75**, 4126 (1995); D. Z. Liu *et al.*, *ibid.* **75**, 4130 (1995); I. I. Mazin and V. M. Yakovenko, *ibid.* **75**, 4134 (1995); L. Yan *et al.*, *ibid.* **78**, 3559 (1997).

[4] B. Friedl *et al.*, Phys. Rev. Lett. **65**, 915 (1990); E. Altendorf *et al.*, Phys. Rev. B **47**, 8140 (1993).

[5] H. A. Mook *et al.*, Phys. Rev. Lett. **65**, 2712 (1990); K. Pyka *et al.*, *ibid.* **70**, 1457 (1993).

[6] R. Zeyher and G. Zwicknagl, Z. Phys. B **78**, 175 (1990); F. Marsiglio, Phys. Rev. B **47**, 5419 (1993); M. E. Flatté, Phys. Rev. Lett. **70**, 658 (1993); C. Jiang and C. Carbotte, Phys. Rev. B **50**, 9449 (1994); A. Bill, V. Hizhnyakov, and E. Sigmund, *ibid.* **52**, 7637 (1995); J. Supercond. **9**, 493 (1996).

[7] B. Normand *et al.*, J. Phys. Soc. Jpn. **64**, 3903 (1995); S. Y. Savrasov and O. K. Andersen, Phys. Rev. Lett. **77**, 4430 (1996).

[8] O. K. Andersen *et al.*, J. Low Temp. Phys. **105**, 285 (1996).

[9] T. P. Devereaux *et al.*, Phys. Rev. B **51**, 505 (1995); Solid State Commun. **108**, 407 (1998).

[10] S. Barišić and I. Batistić, Europhys. Lett. **8**, 765 (1989).

[11] The energy of the upper band follows as

$$\epsilon(\mathbf{k})=s_+(\mathbf{k})+s_-(\mathbf{k})+\epsilon/3,$$

$$s_{\pm}(\mathbf{k}) = [r(\mathbf{k}) \pm \sqrt{q^3(\mathbf{k}) + r^2(\mathbf{k})}]^{1/3},$$

$$q(\mathbf{k}) = -\frac{1}{3}[t_x^2(\mathbf{k}) + t_y^2(\mathbf{k}) + t'^2(\mathbf{k})] - \epsilon^2/9,$$

$$r(\mathbf{k}) = \frac{\epsilon}{6}[t_x^2(\mathbf{k}) + t_y^2(\mathbf{k}) - 2t'^2(\mathbf{k})] - t'(\mathbf{k})t_x(\mathbf{k})t_y(\mathbf{k}) + \epsilon^3/27.$$

Since $q^3(\mathbf{k}) + r^2(\mathbf{k})$ is negative for all $\mathbf{k}$, $s_+^*(\mathbf{k}) = s_-(\mathbf{k})$ and the energy is, of course, real.

[12] T. Fong (private communication).

[13] T. P. Devereaux, Phys. Rev. B **50**, 10 287 (1994).

[14] T. P. Devereaux *et al.*, Phys. Rev. Lett. **72**, 396 (1994); Phys. Rev. B **51**, 16 336 (1995).

[15] See, e.g., G. L. Squires, *Introduction to the Theory of Thermal Neutron Scattering* (Dover, New York, 1996).

[16] $\omega_{B_{1g}}$ is slightly smaller than the value used to fit the B_{1g} Fano profile in Ref. 9. The value for the electric field used is in rough agreement with the value obtained from *ab initio* Hartree-Fock cluster calculations in J. Li and J. Ladik, Solid State Commun. **95**, 35 (1995).